

Generalizable and Animatable 3D Full-Head Gaussian Avatar from a Single Image

Shuling Zhao

CSE, HKUST

szhaoax@connect.ust.hk

Dan Xu

CSE, HKUST

danxu@cse.ust.hk



Figure 1. Given a single input image, our method reconstructs animatable 3D full-head Gaussian avatars in a single forward pass. These avatars provide consistent, high-fidelity 360° view synthesis and support real-time (246 FPS) animation.

Abstract

Building 3D animatable head avatars from a single image is an important yet challenging problem. Existing methods generally collapse under large camera pose variations, compromising the realism of 3D avatars. In this work, we propose a new framework to tackle the novel setting of one-shot 3D full-head animatable avatar reconstruction in a single feed-forward pass, enabling real-time animation and simultaneous 360° rendering views. To facilitate efficient animation control, we model 3D head avatars with Gaussian primitives embedded on the surface of a parametric face model within the UV space. To obtain knowledge of full-head geometry and textures, we leverage rich 3D full-head priors within a pretrained 3D generative adversarial network (GAN) for global full-head feature extraction and multi-view supervision. To increase the fidelity of the 3D reconstruction of the input image, we take advantage of the symmetric nature of the UV space and human faces to fuse local fine-grained input image features with the global full-head textures. Extensive experiments demonstrate the effectiveness of our method, achieving high-quality 3D full-head modeling as well as real-time animation, thereby improving

*the realism of 3D talking avatars.*¹

1. Introduction

3D animatable head avatar creation aims to reconstruct 3D animatable heads from 2D inputs, with widespread applications such as teleconferencing, virtual reality (VR), and augmented reality (AR). Despite the success achieved in 3D head reconstruction from multi-view or monocular videos [31, 45, 59, 62], the requirement for video-specific optimization makes such methods time-consuming. To improve efficiency, some approaches reconstruct 3D heads from a single image in a feed-forward manner [8, 9, 25, 40, 48] using Neural Radiance Fields (NeRF) [29]. Recently, 3D Gaussian Splatting (3DGS) [18] is adopted [6, 12, 14] for its impressive rendering quality and speed.

Despite the advancement made in generalizable one-shot 3D animatable head avatar reconstruction, existing methods generally fail when the rendering views significantly differ from the input camera pose. Trained on large-scale monocular face video datasets [47, 61], which predominantly capture frontal face motions, they can hardly generalize to large

¹<https://shaelyn.github.io/fhavatar/>

side views or even back views, which harms the realism of the reconstructed 3D heads.

To realize efficient avatar animation and full-head modeling at the same time, we introduce a new framework for the novel setting of one-shot 3D full-head animatable avatar creation. To allow for animation control, we generate Gaussian primitives in the UV space of a parametric face model (FLAME [23]) so that Gaussians are rigged to the mesh surface and can move along with it during animation. To obtain knowledge of full-head geometry and textures, inspired by the recent success of 3D generative adversarial networks (GANs) in full-head generation [1, 21], we utilize a pretrained 3D GAN [1] and its feed-forward inversion method [2] to efficiently extract UV space global full-head features from the input image and provide multi-view supervision during training. To overcome the limited reconstruction fidelity of the 3D GAN inversion, we fuse the fine-grained local input image features with the global UV full-head feature. Specifically, we make use of the symmetric nature of human faces and the UV space with a transformer-based feature fusion architecture, making tokens from the global UV map query symmetric positions on the local UV feature maps for input appearances, making full use of the input view. To further improve the 3D visual quality of the reconstructed avatar, we propose a 3D total variation loss that encourages Gaussians to fully cover the whole avatar surface, alleviating hole-like artifacts.

Extensive experiments demonstrate that our framework not only reconstructs 3D full-head avatars that can be viewed in 360°, but also achieves state-of-the-art performance in avatar animation. Our contributions are summarized as follows:

- To the best of our knowledge, this paper is the first to create one-shot animatable 3D full-head Gaussian avatars in a feed-forward manner.
- We build a novel framework that generates Gaussians from the global full-head priors of a pretrained 3D GAN and the local appearance details of the input image in the UV space of a parametric face model, enabling 3D full-head modeling and animation at the same time.
- We perform symmetric feature fusion on the global and local UV feature maps, effectively enhancing the global full-head prior with the local input details for high-fidelity 3D reconstruction.
- Extensive experiments on large-scale video datasets [47, 55] demonstrate that our method not only allows full-head rendering, but also outperforms state-of-the-art approaches in avatar animation, improving the realism of 3D head avatars.

2. Related Work

2D Talking Head Generation. By leveraging powerful 2D generative models [11, 15], promising advancements have

been made in 2D talking head generation by adding motion signals into them. Some works estimate motion in an unsupervised manner, representing it with warping fields described by unsupervised keypoints [16, 36, 38, 56, 57] or latent features [41, 44]. Others adopt pretrained models to predict facial landmarks [13, 27, 52]. However, the lack of 3D face modeling hinders performance, leading to face distortion and identity leakage. Some methods [10, 32, 43] extract 3D Morphable Model (3DMM) [3] parameters to introduce 3D information, but they cannot support arbitrary viewpoint rendering. In contrast, we directly model human heads in 3D to enable free-viewpoint rendering.

Optimization-based 3D Animatable Head Avatar Reconstruction. To achieve free viewpoint rendering, a line of research reconstructs 3D animatable heads from multi-view or monocular videos of a specific person. By optimizing on videos of the same identity, these methods [22, 31, 45, 53, 58, 59, 62] generally achieve high visual quality. However, they require videos with thousands of frames for optimization, which hinders practical use. To reduce the need for lengthy video data, another line of research leverages strong priors from 3D GANs [1, 5, 21, 37] and diffusion models [35]. Some methods [39, 50, 60] generate multi-view data with different motions from a single image and optimize on the generated data. Others perform optimization-based GAN inversion [28, 34, 63] from the input image on pretrained 3D GANs to create animatable 3D heads. However, the required optimization process remains time-consuming. In contrast to these methods, we create one-shot 3D animatable heads in a feed-forward manner, avoiding the cumbersome optimization process.

Generalizable 3D Animatable Head Avatar Reconstruction. To improve the generalizability, 3D head reconstruction from a single image in a single forward pass has gained increasing attention. ROME [19] extends 3DMM [23] meshes to model non-facial parts. With the excellent rendering quality of NeRF [29], some methods [8, 9, 24, 25, 40, 48] incorporate motion features into efficient triplanes [5] for high-fidelity head avatar creation. However, their rendering speed generally remains slow. In recent years, 3DGS [18] is widely leveraged for its extraordinary rendering quality and efficiency. GAGAvatar [6] generates two sets of Gaussians for appearance and expression, respectively, and adds a neural renderer to enhance details. LAM [14] initializes Gaussians on FLAME [23] vertices and generates Gaussian attributes by querying image features through a transformer. However, trained on large monocular video datasets [47, 61], which rarely contain frames of the side and back of the head, these methods generally fail when the rendering viewpoint significantly differs from the input view. On the contrary, by combining full-head priors from a pretrained 3D GAN [1] with the input image features, our method can support renderings in 360°.

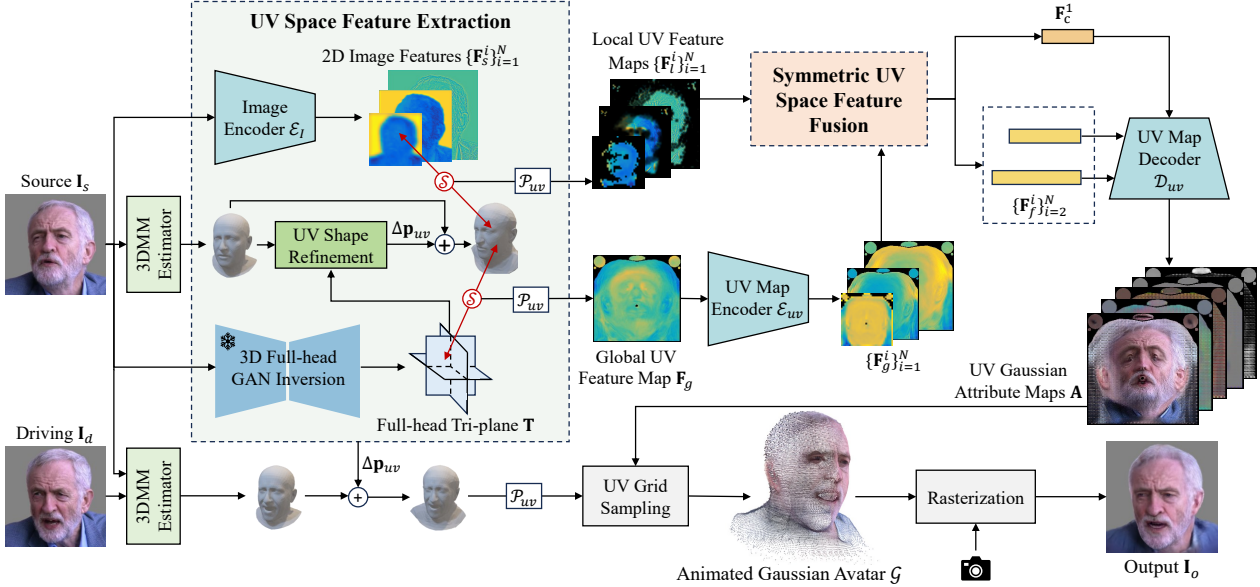


Figure 2. Overview of the framework. Given an input source image, the UV space feature extraction module extracts its global and local UV feature maps for animatable 3D full-head reconstruction. The symmetric UV space feature fusion module takes advantage of the symmetry of human faces and the UV space to combine these UV feature maps. From the predicted UV Gaussian attribute maps, 3D Gaussian primitives are sampled, which can be animated with a parametric face model and rendered given a camera pose.

3. Method

3.1. Overview

Given an input source image of a human face, denoted as \mathbf{I}_s , our goal is to reconstruct an animatable 3D full-head Gaussian avatar on the FLAME [23] mesh surface via UV parameterization. Our framework is illustrated in Fig. 2. First, the UV space feature extraction module extracts the texture features from \mathbf{I}_s and projects them into the UV space, producing a global UV feature map \mathbf{F}_g and multi-scale local UV feature maps $\{\mathbf{F}_l^i\}_{i=1}^N$. It also predicts a shape offset $\Delta\mathbf{p}_{uv}$ to refine the reconstructed FLAME mesh shape based on \mathbf{I}_s . Next, the symmetric UV space feature fusion module takes advantage of the symmetric nature of human faces and the UV space, combining the information from the global and local UV feature maps to generate a set of UV Gaussian attribute maps, from which 3D Gaussian primitives are sampled to reconstruct the Gaussian avatar. Bound to the surface of the source FLAME mesh in canonical space, the Gaussian avatar can be animated with a novel FLAME expression derived from a driving image \mathbf{I}_d and rendered given a camera pose to obtain the output image \mathbf{I}_o . Details on UV space Gaussian modeling, the design of the two modules, the training strategy, and regularization are described in the following subsections.

3.2. UV Space Gaussian Modeling

To utilize the animatable FLAME model for 3D full-head reconstruction and animation, we follow [20, 51] and bind 3D Gaussian primitives to the FLAME mesh surface via UV parameterization, enabling the use of

efficient 2D backbones and regularizing Gaussian positions. Specifically, we generate a UV Gaussian attribute map $\mathbf{A}_\star \in \mathbb{R}^{K \times K \times d_\star}$ for each Gaussian attribute $\star \in \{\text{color, rotation, scale, opacity, position}\}$, where K is the size of the UV map and d_\star is the Gaussian attribute dimension, forming a set of UV Gaussian attribute maps $\mathbf{A} \in \mathbb{R}^{K \times K \times 14}$. Since each valid texel in the UV space already corresponds to a 3D position, we use $\mathbf{p} \in \mathbb{R}^{K \times K \times 3}$ to represent the FLAME-based UV space 3D position map, and $\mathbf{A}_{\text{position}}$ to represent the 3D position offset. To balance the size differences between mesh faces in the UV space and in 3D space, we rescale the UV Gaussian scale map. Specifically, we compute the relative scales between the mesh face sizes on the 3D mesh surface and their corresponding UV face sizes as a relative scaling map $\mathbf{s} \in \mathbb{R}^{K \times K \times 1}$. The UV Gaussian scale map is further updated as $\mathbf{A}_{\text{scale}} = \mathbf{s} \odot \mathbf{A}_{\text{scale}}$, where \odot is the Hadamard product.

To produce 3D Gaussian primitives \mathcal{G} , we perform grid sampling on \mathbf{A} following [20, 51]. The process is formulated as:

$$\mathcal{G} = \text{grid_sample}(\mathbf{A}, \mathcal{X}), \quad (1)$$

where \mathcal{X} is the set of sampling positions in the UV space.

3.3. UV Space Feature Extraction

To generate UV Gaussian attribute maps, we first extract the UV space feature maps from the source image \mathbf{I}_s . The extracted UV feature maps are utilized for later integration.

Full-Head Feature Generation. Since \mathbf{I}_s only provides the head appearance from the source camera view, it is insufficient to reconstruct the full-head appearance using only in-

formation from \mathbf{I}_s . To obtain knowledge from the invisible areas in \mathbf{I}_s , we propose to utilize the full-head prior of a 3D full-head GAN named PanoHead [1] and its feed-forward inversion method [2] to map \mathbf{I}_s to a full-head tri-plane \mathbf{T} , which provides coarse 3D full-head features for \mathbf{I}_s .

UV Shape Refinement. Utilizing the source FLAME mesh predicted by the 3DMM estimator, we can directly sample the tri-plane feature for each 3D position corresponding to a UV space texel, producing a UV tri-plane feature map \mathbf{F}_T^p . However, FLAME meshes often fail to model the shape of the hair, making the 3D position-based feature sampling inaccurate. We propose to use a 2D UNet \mathcal{F}_{refine} to refine the mesh shape. Given \mathbf{F}_T^p and the UV space 3D position map \mathbf{p} , we predict the UV shape offset $\Delta\mathbf{p}_{uv}$ as:

$$\Delta\mathbf{p}_{uv} = \mathcal{F}_{refine}([\mathbf{F}_T^p, \mathbf{p}]), \quad (2)$$

where $[\cdot, \cdot]$ is the concatenation operation. Then, by adding $\Delta\mathbf{p}_{uv}$ to the original 3D position map \mathbf{p} , we obtain a refined 3D position map $\mathbf{p}_r = \mathbf{p} + \Delta\mathbf{p}_{uv}$.

Global UV Feature Extraction. With the refined 3D position map \mathbf{p}_r , we directly sample the full-head tri-plane \mathbf{T} to produce the global UV feature map \mathbf{F}_g . Produced by the pretrained 3D GAN with rich full-head prior knowledge, the tri-plane feature \mathbf{T} contains convincing global head geometry and full-head texture for \mathbf{I}_s . Therefore, \mathbf{F}_g contains a complete full-head representation of \mathbf{I}_s . However, constrained by the latent code dimension of the GAN inversion method and the resolution of the tri-plane, \mathbf{T} cannot faithfully preserve the appearance details of \mathbf{I}_s , and consequently, neither can \mathbf{F}_g . Additional local features from \mathbf{I}_s are needed for high-fidelity avatar reconstruction.

Local UV Feature Extraction. To extract appearance details from \mathbf{I}_s , we use a CNN-based encoder to encode \mathbf{I}_s into multi-scale 2D image features $\{\mathbf{F}_s^i\}_{i=1}^N$. To map the image features to the UV space, we utilize the refined 3D position map \mathbf{p}_r . By projecting the 3D positions in \mathbf{p}_r onto the 2D feature space according to the source camera pose, we can sample the corresponding 2D image feature for each UV texel, resulting in a set of multi-scale UV source features $\{\mathbf{F}_{s,uv}^i\}_{i=1}^N$. However, due to occlusion, only part of the 3D positions in \mathbf{p}_r are visible in the source image. To avoid obtaining mismatched features in the UV space, we filter out invisible 3D positions in \mathbf{p}_r following [17, 46], which results in a UV space visibility mask \mathbf{M}_v . By applying this mask to $\{\mathbf{F}_{s,uv}^i\}_{i=1}^N$, we exclude textures sampled from the invisible positions in the source image. The resulting multi-scale local UV feature maps $\{\mathbf{F}_l^i\}_{i=1}^N$ preserve the local appearance details from \mathbf{I}_s .

3.4. Symmetric UV Space Feature Fusion

In this module, we aim to combine the coarse global UV feature map \mathbf{F}_g with the fine-grained local UV feature maps $\{\mathbf{F}_l^i\}_{i=1}^N$ for UV Gaussian attribute map generation.

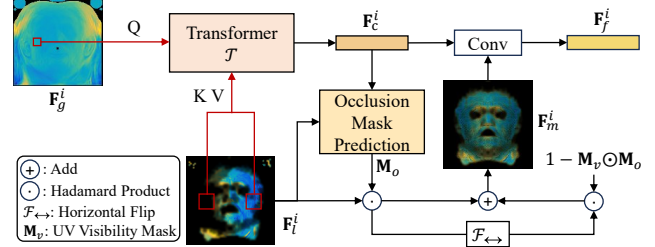


Figure 3. Illustration of Symmetric UV Space Feature Fusion at scale i . For each feature patch in \mathbf{F}_g^i , we query two symmetric local windows corresponding to the patch position in \mathbf{F}_l^i . The output feature \mathbf{F}_c^i is further enhanced by the local UV feature map and its symmetry with convolution.

To better fuse the global UV feature map \mathbf{F}_g and multi-scale local UV feature map $\{\mathbf{F}_l^i\}_{i=1}^N$, we also encode \mathbf{F}_g with a CNN-based UV map encoder to produce multi-scale global UV feature maps $\{\mathbf{F}_g^i\}_{i=1}^N$, and fuse \mathbf{F}_g^i with \mathbf{F}_l^i at scale i across N scales.

Symmetric UV Space Feature Fusion at Scale i . As a global full-head feature, \mathbf{F}_g^i provides plausible texture for each valid texel in the UV space, even for the invisible area in the source view. However, it lacks the appearance details visible in the source image, and we need to transfer such details from \mathbf{F}_l^i to it. Intuitively, \mathbf{F}_g^i and \mathbf{F}_l^i are inherently aligned, as each valid UV texel in \mathbf{F}_g^i and \mathbf{F}_l^i corresponds to the same 3D position on human heads. However, we generate the global and local UV feature maps using 3D position-based sampling and 3D projection, and the 3D positions and projections may still contain errors. To alleviate the potential misalignment issue caused by the errors, inspired by [30], we use a transformer architecture to fuse the features, where \mathbf{F}_g^i serves as the query while \mathbf{F}_l^i serves as the key and value at the cross attention layer. As illustrated in Fig. 3, for each patch token in \mathbf{F}_g^i , we query tokens located in a local window of size $w \times w$ centered at the corresponding patch token in \mathbf{F}_l^i , allowing for small deviations in 3D positions and projections. However, if the source image contains a side view, tokens on the opposite side of the face in the UV space can hardly retrieve useful information from \mathbf{F}_l^i , as its corresponding local window only contains the masked-out area. Essentially, human faces are generally symmetric, and the face UV space is also symmetric. To better utilize the symmetry and retrieve more useful information from \mathbf{F}_l^i , we also use patch tokens in the symmetric local window of \mathbf{F}_l^i as key-value pairs for cross attention.

However, as patchification inevitably leads to information loss, especially for large patches used in large resolution feature maps at large scale i , appearance details contained in $\{\mathbf{F}_l^i\}_{i=2}^N$ may not be fully transferred to the transformer outputs $\{\mathbf{F}_c^i\}_{i=2}^N$. To further enhance appearance details from $\{\mathbf{F}_l^i\}_{i=2}^N$ within the aligned areas, we predict an occlusion mask \mathbf{M}_o based on \mathbf{F}_c^i and \mathbf{F}_l^i to mask out the

region of erroneous 3D projections in \mathbf{F}_l^i , producing a more accurate local feature $\mathbf{F}_{l,m}^i$:

$$\mathbf{F}_{l,m}^i = \mathbf{M}_o \odot \mathbf{F}_l^i, \quad (3)$$

where \odot is the Hadamard product. To utilize the symmetric nature of faces and the UV space, we horizontally flip the masked $\mathbf{F}_{l,m}^i$ and add it to the masked-out area in $\mathbf{F}_{l,m}^i$, taking full advantage of the appearance information from \mathbf{F}_l^i . The output \mathbf{F}_m^i is further fused with \mathbf{F}_c^i with a convolution layer to produce the final \mathbf{F}_f^i . The process is formulated as:

$$\mathbf{F}_m^i = \mathbf{F}_{l,m}^i + \mathcal{F}_{\leftrightarrow}(\mathbf{F}_{l,m}^i) \odot (1 - \mathbf{M}_v \odot \mathbf{M}_o), \quad (4)$$

$$\mathbf{F}_f^i = \text{Conv}([\mathbf{F}_c^i, \mathbf{F}_m^i]), \quad (5)$$

where $\mathcal{F}_{\leftrightarrow}$ is the horizontal flip operation, \odot is the Hadamard product, and $[\cdot, \cdot]$ is the concatenation operation.

UV Gaussian Attribute Map Generation. We generate the set of UV Gaussian attribute maps \mathbf{A} with the UV map decoder \mathcal{D}_{uv} and the fused UV features \mathbf{F}_c^1 and $\{\mathbf{F}_f^i\}_{i=2}^N$. We use the transformer output \mathbf{F}_c^1 instead of \mathbf{F}_f^1 , as \mathbf{F}_f^1 has the smallest resolution and contains few appearance details. \mathbf{F}_c^1 serves as the initial input to \mathcal{D}_{uv} , where it is gradually upsampled and processed with residual blocks. $\{\mathbf{F}_f^i\}_{i=2}^N$ is added to the intermediate feature maps with the same size in \mathcal{D}_{uv} . The final output of \mathcal{D}_{uv} is \mathbf{A} . We also generate another attribute map \mathbf{A}^1 only using \mathbf{F}_c^1 as the input, which is also used to sample Gaussian attributes \mathcal{G} and render an output image \mathbf{I}_o^1 during training, preventing \mathcal{D}_{uv} from relying too much on high-resolution inputs.

3.5. Regularization and Training Strategy

3D Total Variation Loss. As shown in Fig. 4, we observe that Gaussian primitives modeled on the FLAME mesh surface normally cannot cover the whole avatar surface, resulting in holes that make the Gaussians representing the opposite side of the head visible, which harms 3D reconstruction quality. To alleviate such artifacts, inspired by the UV total variation (TV) loss in [20] that uses TV loss on the UV renderings \mathbf{I}_{uv} rendered from the same Gaussians \mathcal{G} but with \mathcal{G}_{color} set to the UV coordinates, we propose to use the TV loss on the 3D renderings \mathbf{I}_{3d} , which is more suitable for the UV space definitions where neighboring pixels in the rendered image can be far from each other in the UV space (e.g., eyeballs and eyelids). Specifically, based on the sampled Gaussians \mathcal{G} , we change the value of \mathcal{G}_{color} to $\mathcal{G}_{position}$ while leaving other Gaussian attributes unchanged, and perform rendering to obtain the 3D rendering \mathbf{I}_{3d} . The 3D total variation loss is defined as:

$$\mathcal{L}_{3d} = \text{TV}\left(\frac{\mathbf{I}_{3d} - (1 - \mathbf{I}_{\alpha})}{\mathbf{I}_{\alpha}}\right), \quad (6)$$

where \mathbf{I}_{α} is the rendered alpha map. This regularization encourages neighboring pixels in the rendered image to be rendered from neighboring Gaussians in the 3D space.

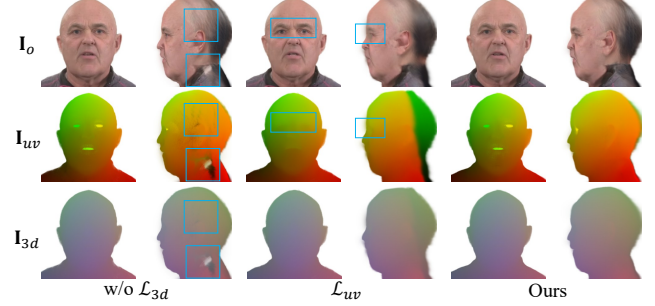


Figure 4. Effect of the 3D total variation loss \mathcal{L}_{3d} . Compared with the UV total variation loss \mathcal{L}_{uv} from [20], \mathcal{L}_{3d} can alleviate holes on the avatar surfaces without bringing additional artifacts. Blue boxes indicate the erroneous areas in the rendered images.

Training Strategy. Except the offline 3DMM estimator and the frozen pretrained 3D full-head GAN and its inversion, we train the whole framework end-to-end. During training, we randomly sample two frames from a video of the same identity, in which one frame serves as the source image and the other serves as the driving image. With the source image \mathbf{I}_s and the 3DMM motion parameter from the driving image \mathbf{I}_d , we aim to reconstruct the target image, which is \mathbf{I}_d . As large-scale face video datasets generally contain frontal faces, we rely on the pretrained 3D full-head GAN and its inversion to generate pseudo multi-view images of \mathbf{I}_d for supervision. However, we find that the inversion method tends to generate inconsistent invisible parts of the head given different frames of a video, providing inconsistent multi-view supervision for different \mathbf{I}_d given the same \mathbf{I}_s , which may hamper the 3D reconstruction quality. Therefore, we follow [8] to randomly switch between the animation mode and the 3D reconstruction mode. Specifically, in animation mode, we use \mathbf{I}_s as the source image and \mathbf{I}_d as the target image. In 3D reconstruction mode, we use \mathbf{I}_d as the source image, \mathbf{I}_d together with its inverted novel views as the target images to avoid the inconsistency in the pseudo supervision.

For the training objective, we render RGB images \mathbf{I}_o and \mathbf{I}_o^1 , alpha maps \mathbf{I}_{α} and \mathbf{I}_{α}^1 from \mathcal{G} and \mathcal{G}^1 , respectively. We supervise the RGB images using the target image(s) with a reconstruction loss $\mathcal{L}_{re} = \mathcal{L}_1 + \mathcal{L}_{lpips}$, and supervise the alpha maps with \mathcal{L}_1 loss, denoted as \mathcal{L}_{α} . When \mathbf{I}_o contains frontal faces, we also use an ID similarity loss [7] \mathcal{L}_{id} .

Apart from the 3D total variation loss, we also apply a series of regularizations to constrain the Gaussian primitives for better rendering quality. Following [51], we apply the eyeball TV loss \mathcal{L}_{eye} and the position offset regularization $\mathcal{L}_{pos} = \|\mathbf{A}_{position}\|_2$. To limit the extent of FLAME mesh offset, we regularize the predicted UV shape offset $\Delta \mathbf{p}_{uv}$:

$$\mathcal{L}_{shape} = \max(\|\Delta \mathbf{p}_{uv}\|_2 - \epsilon, 0), \quad (7)$$

where ϵ is a threshold. To avoid producing Gaussian out-

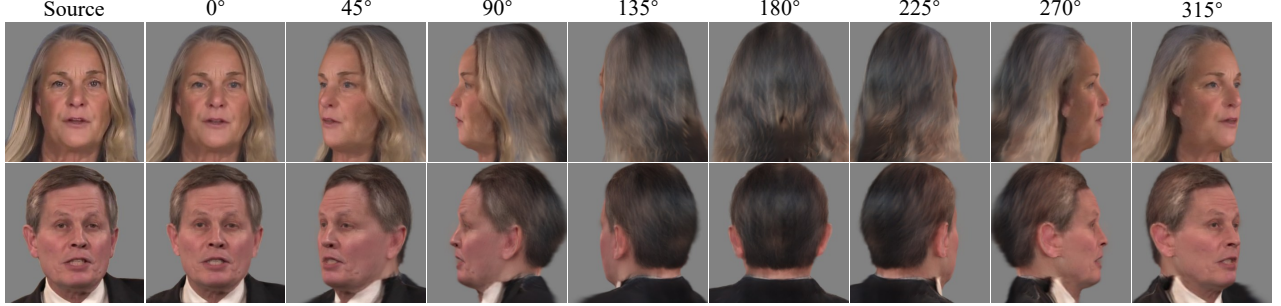


Figure 5. Multi-view results of our method on the HDTF [55] dataset. Our avatars can be viewed in 360°.

Method	Self-reenactment							Cross-identity Reenactment		
	PSNR \uparrow	SSIM \uparrow	LPIPS \downarrow	CSIM \uparrow	AKD \downarrow	AED \downarrow	APD \downarrow	CSIM \uparrow	AED \downarrow	APD \downarrow
StyleHEAT [49]	18.96	0.7505	0.3821	0.1695	20.78	0.7236	4.1380	0.1096	0.8195	3.3018
GOHA [25]	19.87	0.7322	0.2769	0.6469	3.746	0.4279	1.0326	0.4712	0.6859	1.9107
Real3DPortrait [48]	21.00	0.7572	0.2915	0.7696	3.934	0.3918	1.1890	0.6562	0.7186	1.7875
Portrait4D [8]	16.94	0.6621	0.4597	0.7339	19.77	0.4111	1.6261	0.5806	0.7323	2.2870
Portrait4D-v2 [9]	17.65	0.6790	0.3674	0.8070	19.29	0.3542	1.4282	0.6731	0.6619	2.2236
GAGAvatar [6]	21.60	0.7745	0.2249	0.8459	2.954	0.3125	0.8898	0.6681	0.6409	1.7486
LAM [14]	21.67	0.7756	0.2716	0.6846	3.676	0.4535	1.4286	0.5562	0.7271	3.2028
Ours	23.24	0.7995	0.2384	0.8012	2.798	0.3634	0.8660	0.6757	0.7103	2.3661

Table 1. Quantitative comparison with state-of-the-art methods on the VFHQ dataset [47].

liers, we further add a TV regularization to $\Delta \mathbf{p}_{uv}$:

$$\mathcal{L}_{shape}^{tv} = TV(\Delta \mathbf{p}_{uv}). \quad (8)$$

Thus, our regularization is defined as:

$$\begin{aligned} \mathcal{L}_{reg} = & \lambda_{3d} \mathcal{L}_{3d} + \lambda_{eye} \mathcal{L}_{eye} + \lambda_{pos} \mathcal{L}_{pos} \\ & + \lambda_{shape} \mathcal{L}_{shape} + \lambda_{shape}^{tv} \mathcal{L}_{shape}^{tv}, \end{aligned} \quad (9)$$

where λ_* is the regularization weight.

To summarize, our training objective is:

$$\mathcal{L} = \mathcal{L}_{re} + \mathcal{L}_{\alpha} + \lambda_{id} \mathcal{L}_{id} + \lambda^1 (\mathcal{L}_{lpips}^1 + \mathcal{L}_{\alpha}^1) + \mathcal{L}_{reg}, \quad (10)$$

where λ_{id} and λ^1 are the loss weights, and \mathcal{L}_{lpips}^1 and \mathcal{L}_{α}^1 denote the losses for \mathbf{I}_o^1 and \mathbf{I}_{α}^1 , respectively.

4. Experiments

4.1. Experimental Setup

Datasets. We train our model on the VFHQ dataset [47]. For data preprocessing, we follow [1, 2] to estimate the camera pose, crop and remove the background of each video frame. All frames are resized to 512×512 . To obtain the FLAME parameters, we utilize the head tracker from [31]. For performance evaluation, we use the VFHQ test split. To evaluate the generalizability, we randomly sample 20 videos from HDTF dataset [55] following [6, 14]. We also sample 21 videos from a multi-view MEAD [42] video dataset to assess the effectiveness of our design under large camera pose changes.

Metrics. For self-reenactment, given ground-truth frames, we use PSNR, SSIM, LPIPS [54] to evaluate the reconstruction quality. For identity preservation, we use cosine

similarity (CSIM) of identity features extracted by [7]. For driving accuracy, we use average keypoint distance (AKD) based on [4], average expression distance (AED) based on [33] and average pose distance (APD) based on [26]. For the setting of cross-identity reenactment, with no ground-truth available, we use CSIM, AED and APD for evaluation, following prior works [6, 14].

4.2. Comparison with State-of-the-art Methods

We compare with 2D-based StyleHEAT [49], and 3D-based GOHA [25], Real3DPortrait [48], Portrait4D [8], Portrait4D-v2 [9], GAGAvatar [6] and LAM [14].

Quantitative Comparison. We present the results of the quantitative comparison with state-of-the-art methods on the VFHQ [47] and HDTF [55] datasets in Tab. 1 and Tab. 2. For self-reenactment, we use the first frame of each video as the source image and the rest as the driving images. For cross-identity reenactment, we randomly sample a frame from the video of a different identity as the source image. Our method generally achieves the best performance for self-reenactment and remains competitive for cross-identity reenactment. In terms of reconstruction quality (*i.e.*, PSNR, SSIM), our method significantly outperforms previous methods on both datasets, highlighting the effectiveness of symmetric UV space feature fusion, where appearance details from the input source image are combined for Gaussian attribute map generation. Our method also achieves the best AKD and APD for self-reenactment, which confirms the accuracy of expression and pose during animation. For cross-identity reenactment, our method outperforms others in identity preservation on the VFHQ dataset, where large differences in camera pose between

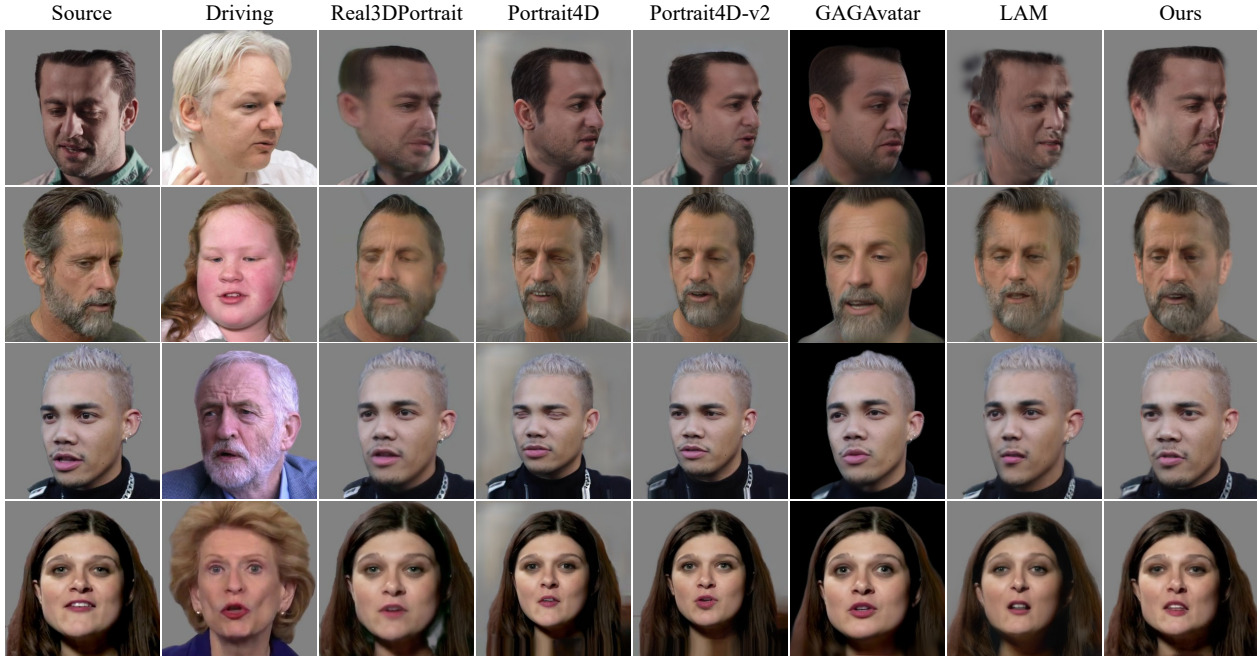


Figure 6. Qualitative comparison with state-of-the-art methods (*i.e.*, Real3DPortrait [48], Portrait4D [8], Portrait4D-v2 [9], GAGAvatar [6] and LAM [14]) for cross-identity reenactment on the VFHQ [47] and HDTF [55] datasets. Our method best maintains source identity while effectively mimicking the driving motion.

Method	Self-reenactment							Cross-identity Reenactment		
	PSNR \uparrow	SSIM \uparrow	LPIPS \downarrow	CSIM \uparrow	AKD \downarrow	AED \downarrow	APD \downarrow	CSIM \uparrow	AED \downarrow	APD \downarrow
StyleHEAT [49]	21.91	0.8102	0.2979	0.5096	6.564	0.4860	1.1539	0.4624	0.7656	1.4266
GOHA [25]	21.33	0.7739	0.2436	0.7541	3.164	0.4128	0.7296	0.7471	0.7287	1.2370
Real3DPortrait [48]	23.39	0.8110	0.2362	0.8570	3.104	0.3413	0.7633	0.8886	0.7487	1.1770
Portrait4D [8]	20.03	0.7462	0.3602	0.8049	8.390	0.3787	1.1614	0.7873	0.7482	1.4098
Portrait4D-v2 [9]	20.86	0.7581	0.2638	0.8640	8.400	0.3398	1.1432	0.8669	0.7332	1.3919
GAGAvatar [6]	23.72	0.8177	0.2089	0.8894	2.679	0.3034	0.5977	0.9004	0.7300	1.2045
LAM [14]	23.55	0.8167	0.2362	0.7542	3.386	0.4180	0.8911	0.7656	0.7731	1.6635
Ours	26.61	0.8642	0.1900	0.8622	2.287	0.3318	0.5286	0.8568	0.7347	1.5605

Table 2. Quantitative comparison with state-of-the-art methods on the HDTF dataset [55].

source and driving image pairs occur most frequently. This indicates the superiority of modeling 3D full heads. In terms of motion accuracy for cross-identity reenactment, we achieve slightly worse AED and APD. Based on the motion from the tracked FLAME parameters, the expression and pose accuracy of our method is limited by the tracking accuracy. Nevertheless, for AED and APD scores, our method outperforms LAM [14], which shares the same FLAME head tracker with us.

Qualitative Comparison. Fig. 6 shows qualitative comparison results with state-of-the-art methods. Our method can maintain the source face identity better than previous methods under large camera pose changes (row 1 and 2) while imitating the driving expressions accurately (row 3 and 4), which confirms the importance of 3D full-head reconstruction during animation. The 360° rendering results of the avatars reconstructed by our method in Fig. 5 confirm the effectiveness of our UV space full-head modeling, allowing for more realistic 3D avatars. More qualitative comparison

results are shown in the supplementary material.

Inference Speed. Tab. 4 measures the time of reenactment during inference using an NVIDIA RTX 3090. Based on the efficient 3DGS representation, our method achieves an FPS of 246, outperforming previous methods. This confirms the efficiency of our method and highlights its potential real-time applications.

4.3. Ablation Study

We perform ablation studies to analyze the effectiveness of our framework design. The quantitative comparison is presented in Tab. 3 and the qualitative results are shown in Fig. 7 and Fig. 4.

UV Shape Refinement. According to Tab. 3, removing UV shape refinement (w/o Δp_{uv}) degrades the overall performance, as we cannot obtain a more accurate 3D position to sample the appropriate features from the full-head tri-plane and the 2D image features. Fig. 7 shows clear boundary artifacts and blurry hair in the rendered frames without UV

Method	HDTF							MEAD						
	PSNR \uparrow	SSIM \uparrow	LPIPS \downarrow	CSIM \uparrow	AKD \downarrow	AED \downarrow	APD \downarrow	PSNR \uparrow	SSIM \uparrow	LPIPS \downarrow	CSIM \uparrow	AKD \downarrow	AED \downarrow	APD \downarrow
w/o Δp_{uv}	26.15	0.8596	0.2058	0.8618	2.338	0.3321	0.5751	17.09	0.7495	0.3493	0.6678	5.887	0.5032	2.6566
w/o $\{\mathbf{F}_l^i\}_{i=1}^N$	23.82	0.8186	0.2658	0.5230	2.732	0.3986	0.7115	17.09	0.7508	0.3541	0.3932	4.849	0.6903	1.9517
w/o \mathcal{T}	25.79	0.8579	0.2049	0.8461	2.335	0.3443	0.5831	17.05	0.7468	0.3430	0.6500	4.792	0.5044	2.1080
w/o Sym.	26.60	0.8651	0.1893	0.8646	2.307	0.3402	0.5587	17.18	0.7475	0.3402	0.6631	5.103	0.5047	2.2145
\mathcal{L}_{uv}	26.40	0.8622	0.1911	0.8567	2.324	0.3447	0.5370	17.08	0.7459	0.3458	0.6663	5.058	0.4806	1.9627
Ours	26.61	0.8642	0.1900	0.8622	2.287	0.3318	0.5286	17.20	0.7495	0.3402	0.6765	4.844	0.5037	1.9484

Table 3. Ablation study on the design of our framework. We present the results for self-reenactment on the HDTF [55] and multi-view MEAD [42] datasets. Our complete design achieves consistently the best results on both datasets.

Method	StyleHEAT [49]	GOHA [25]	Real3DPortrait [48]	Portrait4D-v2 [9]	GAGAvatar [6]	LAM [14]	Ours
FPS	2.19	4.91	11.02	18.39	58.11	231.74	246.00

Table 4. Inference speed measured in FPS. All results exclude the time for source avatar reconstruction and driving motion extraction that can be calculated beforehand. We take an average over 100 frames.

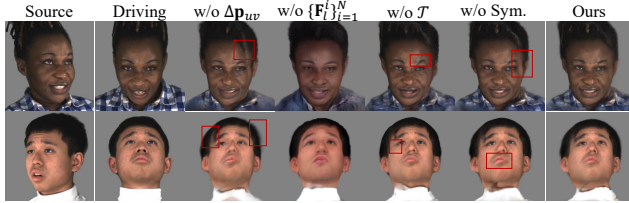


Figure 7. Qualitative ablation study on the MEAD [42] dataset. Our method performs best under large pose changes.

shape refinement.

Local UV Feature Maps. Tab. 3 and Fig. 7 show that we can hardly preserve the identity from the input source image without using local UV feature maps (w/o $\{\mathbf{F}_l^i\}_{i=1}^N$), with a significant drop in CSIM. Although the full-head tri-plane is inverted from the source image, it cannot preserve appearance details, as the dimension of the inverted latent code and the tri-plane resolution are limited. We cannot reconstruct faithful 3D head avatars without using local UV feature maps.

Symmetric UV Space Feature Fusion. We utilize a transformer-based UV feature fusion strategy with symmetry prior. We analyze its effectiveness by removing the transformer (w/o \mathcal{T}) and removing symmetric operations (w/o Sym.) respectively.

When the transformer is removed, the symmetric local UV features are directly fused with the global UV features without filtering out potential errors in 3D projection, which decreases the overall performance as shown in Tab. 3. We can observe that the eyebrow is distorted and artifacts appear at the eye in Fig. 7, which is caused by inaccurate 3D projections at face boundaries.

After we remove the symmetric operations, the quantitative results in Tab. 3 are still comparable with the full design on HDTF, but they generally drop when evaluated on the multi-view MEAD dataset. Since the symmetric operations take the most effect when only a side face is visible in the source image, they cannot contribute significantly to the final results given the videos with frontal faces in HDTF.

Nevertheless, they can generally improve full-head avatar animation quality on the multi-view video dataset where source and driving camera poses may vary significantly. According to Fig. 7, the symmetric operation reduces artifacts at the source face boundaries, improving the reconstruction quality of the invisible parts in the source images.

3D Total Variation Loss. As shown in Fig. 4, without using the 3D total variation loss (w/o \mathcal{L}_{3d}), the generated Gaussians cannot cover the avatar surface, leaving holes on the reconstructed avatars, which greatly harms the 3D quality.

Using the UV total variation loss (\mathcal{L}_{uv}) from [20] instead of \mathcal{L}_{3d} can also encourage the Gaussians to cover the avatar surface, as \mathcal{L}_{uv} encourages neighboring pixels in the rendered image to be from neighboring texels in the UV space. However, we use a different UV parametrization where eyeballs and inner mouth are far from the eyelid and lip areas in the UV space for full head modeling. Therefore, as shown in Fig. 4, directly using \mathcal{L}_{uv} leads to artifacts in the eye and mouth areas, causing Gaussians bound to other face areas to cover the eyeballs and mouth, which harms the avatar animation quality. The degradation is also confirmed by the quantitative results in Tab. 3. In contrast, using our \mathcal{L}_{3d} can realize a 3D consistent full-head avatar without damaging the animation quality.

5. Conclusion

In this paper, we have tackled a novel setting of building a one-shot 3D full-head animatable avatar in a feed-forward manner, which allows for more immersive 3D talking heads. We propose a novel framework that generates the Gaussian primitives in the UV space of a parametric head model for animation control. We leverage the rich 3D full-head prior knowledge from a pretrained 3D GAN, and perform symmetric UV space feature fusion on the extracted global full-head features together with the fine-grained local image features from the input image, effectively improving the 3D reconstruction fidelity. Extensive experiments confirm the effectiveness of our method, generating 3D head avatars that can be animated and viewed in 360°.

References

[1] Sizhe An, Hongyi Xu, Yichun Shi, Guoxian Song, Umit Y Ogras, and Linjie Luo. Panohead: Geometry-aware 3d full-head synthesis in 360deg. In *CVPR*, 2023. 2, 4, 6

[2] Bahri Batuhan Bilecen, Ahmet Gökmen, and Aysegul Dundar. Dual encoder gan inversion for high-fidelity 3d head reconstruction from single images. In *NeurIPS*, 2024. 2, 4, 6

[3] Volker Blanz and Thomas Vetter. A morphable model for the synthesis of 3d faces. In *SIGGRAPH*, 1999. 2

[4] Adrian Bulat and Georgios Tzimiropoulos. How far are we from solving the 2d & 3d face alignment problem?(and a dataset of 230,000 3d facial landmarks). In *ICCV*, 2017. 6

[5] Eric R Chan, Connor Z Lin, Matthew A Chan, Koki Nagano, Boxiao Pan, Shalini De Mello, Orazio Gallo, Leonidas J Guibas, Jonathan Tremblay, Sameh Khamis, et al. Efficient geometry-aware 3d generative adversarial networks. In *CVPR*, 2022. 2

[6] Xuangeng Chu and Tatsuya Harada. Generalizable and animatable gaussian head avatar. In *NeurIPS*, 2024. 1, 2, 6, 7, 8, 3

[7] Jiankang Deng, Jia Guo, Niannan Xue, and Stefanos Zafeiriou. Arcface: Additive angular margin loss for deep face recognition. In *CVPR*, 2019. 5, 6

[8] Yu Deng, Duomin Wang, Xiaohang Ren, Xingyu Chen, and Baoyuan Wang. Portrait4d: Learning one-shot 4d head avatar synthesis using synthetic data. In *CVPR*, 2024. 1, 2, 5, 6, 7, 3

[9] Yu Deng, Duomin Wang, and Baoyuan Wang. Portrait4d-v2: Pseudo multi-view data creates better 4d head synthesizer. In *ECCV*, 2024. 1, 2, 6, 7, 8, 3

[10] Michail Christos Doukas, Stefanos Zafeiriou, and Viktoriia Sharmanska. Headgan: One-shot neural head synthesis and editing. In *ICCV*, 2021. 2

[11] Ian J Goodfellow, Jean Pouget-Abadie, Mehdi Mirza, Bing Xu, David Warde-Farley, Sherjil Ozair, Aaron Courville, and Yoshua Bengio. Generative adversarial nets. In *NeurIPS*, 2014. 2

[12] Chen Guo, Zhuo Su, Jian Wang, Shuang Li, Xu Chang, Zhaohu Li, Yang Zhao, Guidong Wang, and Ruqi Huang. Sega: Drivable 3d gaussian head avatar from a single image. *arXiv preprint arXiv:2504.14373*, 2025. 1

[13] Sungjoo Ha, Martin Kersner, Beomsu Kim, Seokjun Seo, and Dongyoung Kim. Marionette: Few-shot face reenactment preserving identity of unseen targets. In *AAAI*, 2020. 2

[14] Yisheng He, Xiaodong Gu, Xiaodan Ye, Chao Xu, Zhengyi Zhao, Yuan Dong, Weihao Yuan, Zilong Dong, and Liefeng Bo. Lam: Large avatar model for one-shot animatable gaussian head. In *SIGGRAPH*, 2025. 1, 2, 6, 7, 8, 3

[15] Jonathan Ho, Ajay Jain, and Pieter Abbeel. Denoising diffusion probabilistic models. In *NeurIPS*, 2020. 2

[16] Fa-Ting Hong, Longhao Zhang, Li Shen, and Dan Xu. Depth-aware generative adversarial network for talking head video generation. In *CVPR*, 2022. 2

[17] Shoukang Hu, Fangzhou Hong, Liang Pan, Haiyi Mei, Lei Yang, and Ziwei Liu. Sherf: Generalizable human nerf from a single image. In *ICCV*, 2023. 4

[18] Bernhard Kerbl, Georgios Kopanas, Thomas Leimkühler, and George Drettakis. 3d gaussian splatting for real-time radiance field rendering. *ACM TOG*, 42(4):139–1, 2023. 1, 2

[19] Taras Khakhulin, Vanessa Sklyarova, Victor Lempitsky, and Egor Zakharov. Realistic one-shot mesh-based head avatars. In *ECCV*, 2022. 2

[20] Tobias Kirschstein, Simon Giebenhain, Jiapeng Tang, Markos Georgopoulos, and Matthias Nießner. Gghead: Fast and generalizable 3d gaussian heads. In *SIGGRAPH Asia*, 2024. 3, 5, 8

[21] Heyuan Li, Ce Chen, Tianhao Shi, Yuda Qiu, Sizhe An, Guanying Chen, and Xiaoguang Han. Spherehead: stable 3d full-head synthesis with spherical tri-plane representation. In *ECCV*, 2024. 2

[22] Linzhou Li, Yumeng Li, Yanlin Weng, Youyi Zheng, and Kun Zhou. Rgbavatar: Reduced gaussian blendshapes for online modeling of head avatars. In *CVPR*, 2025. 2

[23] Tianye Li, Timo Bolkart, Michael J Black, Hao Li, and Javier Romero. Learning a model of facial shape and expression from 4d scans. *ACM TOG*, 36(6):1–17, 2017. 2, 3, 1

[24] Weichuang Li, Longhao Zhang, Dong Wang, Bin Zhao, Zhi-gang Wang, Mulin Chen, Bang Zhang, Zhongjian Wang, Liefeng Bo, and Xuelong Li. One-shot high-fidelity talking-head synthesis with deformable neural radiance field. In *CVPR*, 2023. 2

[25] Xueting Li, Shalini De Mello, Sifei Liu, Koki Nagano, Umar Iqbal, and Jan Kautz. Generalizable one-shot 3d neural head avatar. In *NeurIPS*, 2023. 1, 2, 6, 7, 8

[26] Camillo Lugaressi, Jiuqiang Tang, Hadon Nash, Chris Mc-Clanahan, Esha Ubweja, Michael Hays, Fan Zhang, Chuo-Ling Chang, Ming Guang Yong, Juhyun Lee, et al. Mediapipe: A framework for building perception pipelines. *arXiv preprint arXiv:1906.08172*, 2019. 6

[27] Yue Ma, Hongyu Liu, Hongfa Wang, Heng Pan, Yingqing He, Junkun Yuan, Ailing Zeng, Chengfei Cai, Heung-Yeung Shum, Wei Liu, et al. Follow-your-emoji: Fine-controllable and expressive freestyle portrait animation. In *SIGGRAPH Asia*, 2024. 2

[28] Zhiyuan Ma, Xiangyu Zhu, Guo-Jun Qi, Zhen Lei, and Lei Zhang. Ottavator: One-shot talking face avatar with controllable tri-plane rendering. In *CVPR*, 2023. 2

[29] Ben Mildenhall, Pratul P Srinivasan, Matthew Tancik, Jonathan T Barron, Ravi Ramamoorthi, and Ren Ng. Nerf: Representing scenes as neural radiance fields for view synthesis. In *ECCV*, 2020. 1, 2

[30] Panwang Pan, Zhuo Su, Chenguo Lin, Zhen Fan, Yongjie Zhang, Zeming Li, Tingting Shen, Yadong Mu, and Yebin Liu. Humansplat: Generalizable single-image human gaussian splatting with structure priors. In *NeurIPS*, 2024. 4

[31] Shenhan Qian, Tobias Kirschstein, Liam Schoneveld, Davide Davoli, Simon Giebenhain, and Matthias Nießner. Gaussianavatars: Photorealistic head avatars with rigged 3d gaussians. In *CVPR*, 2024. 1, 2, 6

[32] Yurui Ren, Ge Li, Yuanqi Chen, Thomas H. Li, and Shan Liu. Pirenderer: Controllable portrait image generation via semantic neural rendering. In *ICCV*, 2021. 2

[33] George Retsinas, Panagiotis P Filntisis, Radek Danecek, Victoria F Abrevaya, Anastasios Roussos, Timo Bolkart, and Petros Maragos. 3d facial expressions through analysis-by-neural-synthesis. In *CVPR*, 2024. 6

[34] Daniel Roich, Ron Mokady, Amit H Bermano, and Daniel Cohen-Or. Pivotal tuning for latent-based editing of real images. *ACM TOG*, 42(1):1–13, 2022. 2

[35] Robin Rombach, Andreas Blattmann, Dominik Lorenz, Patrick Esser, and Björn Ommer. High-resolution image synthesis with latent diffusion models. In *CVPR*, 2022. 2

[36] Aliaksandr Siarohin, Stéphane Lathuilière, Sergey Tulyakov, Elisa Ricci, and Nicu Sebe. First order motion model for image animation. In *NeurIPS*, 2019. 2

[37] Jingxiang Sun, Xuan Wang, Lizhen Wang, Xiaoyu Li, Yong Zhang, Hongwen Zhang, and Yebin Liu. Next3d: Generative neural texture rasterization for 3d-aware head avatars. In *CVPR*, 2023. 2

[38] Jiale Tao, Shuhang Gu, Wen Li, and Lixin Duan. Learning motion refinement for unsupervised face animation. In *NeurIPS*, 2024. 2

[39] Felix Taubner, Ruihang Zhang, Mathieu Tuli, and David B Lindell. Cap4d: Creating animatable 4d portrait avatars with morphable multi-view diffusion models. In *CVPR*, 2025. 2

[40] Phong Tran, Egor Zakharov, Long-Nhat Ho, Anh Tuan Tran, Liwen Hu, and Hao Li. Voodoo 3d: Volumetric portrait disentanglement for one-shot 3d head reenactment. In *CVPR*, 2024. 1, 2

[41] Duomin Wang, Yu Deng, Zixin Yin, Heung-Yeung Shum, and Baoyuan Wang. Progressive disentangled representation learning for fine-grained controllable talking head synthesis. In *CVPR*, 2023. 2

[42] Kaisiyuan Wang, Qianyi Wu, Linsen Song, Zhuoqian Yang, Wayne Wu, Chen Qian, Ran He, Yu Qiao, and Chen Change Loy. Mead: A large-scale audio-visual dataset for emotional talking-face generation. In *ECCV*, 2020. 6, 8

[43] Qiulin Wang, Lu Zhang, and Bo Li. Safa: Structure aware face animation. In *3DV*, 2021. 2

[44] Yaohui Wang, Di Yang, Francois Bremond, and Antitza Dantcheva. Latent image animator: Learning to animate images via latent space navigation. In *ICLR*, 2022. 2

[45] Jun Xiang, Xuan Gao, Yudong Guo, and Juyong Zhang. Flashavatar: High-fidelity head avatar with efficient gaussian embedding. In *CVPR*, 2024. 1, 2

[46] Jiaxin Xie, Hao Ouyang, Jingtian Piao, Chenyang Lei, and Qifeng Chen. High-fidelity 3d gan inversion by pseudo multi-view optimization. In *CVPR*, 2023. 4

[47] Liangbin Xie, Xintao Wang, Honglun Zhang, Chao Dong, and Ying Shan. Vfhq: A high-quality dataset and benchmark for video face super-resolution. In *CVPRW*, 2022. 1, 2, 6, 7, 3

[48] Zhenhui Ye, Tianyun Zhong, Yi Ren, Jiaqi Yang, Weichuang Li, Jiawei Huang, Ziyue Jiang, Jinzheng He, Rongjie Huang, Jinglin Liu, Chen Zhang, Xiang Yin, Zejun MA, and Zhou Zhao. Real3d-portrait: One-shot realistic 3d talking portrait synthesis. In *ICLR*, 2024. 1, 2, 6, 7, 8, 3

[49] Fei Yin, Yong Zhang, Xiaodong Cun, Mingdeng Cao, Yanbo Fan, Xuan Wang, Qingyan Bai, Baoyuan Wu, Jue Wang, and Yujiu Yang. Styleheat: One-shot high-resolution editable talking face generation via pre-trained stylegan. In *ECCV*, 2022. 6, 7, 8, 1

[50] Fei Yin, Chun-Han Yao, Rafal K Mantiuk, Varun Jampani, et al. Facecraft4d: Animated 3d facial avatar generation from a single image. In *ICCV*, 2025. 2

[51] Zhengming Yu, Tianye Li, Jingxiang Sun, Omer Shapira, Seonwook Park, Michael Stengel, Matthew Chan, Xin Li, Wenping Wang, Koki Nagano, et al. Gaia: Generative animatable interactive avatars with expression-conditioned gaussians. In *SIGGRAPH*, 2025. 3, 5

[52] Egor Zakharov, Aleksei Ivakhnenko, Aliaksandra Shysheya, and Victor Lempitsky. Fast bi-layer neural synthesis of one-shot realistic head avatars. In *ECCV*, 2020. 2

[53] Jiawei Zhang, Zijian Wu, Zhiyang Liang, Yicheng Gong, Dongfang Hu, Yao Yao, Xun Cao, and Hao Zhu. Fate: Full-head gaussian avatar with textural editing from monocular video. In *CVPR*, 2025. 2

[54] Richard Zhang, Phillip Isola, Alexei A Efros, Eli Shechtman, and Oliver Wang. The unreasonable effectiveness of deep features as a perceptual metric. In *CVPR*, 2018. 6

[55] Zhimeng Zhang, Lincheng Li, Yu Ding, and Changjie Fan. Flow-guided one-shot talking face generation with a high-resolution audio-visual dataset. In *CVPR*, 2021. 2, 6, 7, 8, 3

[56] Jian Zhao and Hui Zhang. Thin-plate spline motion model for image animation. In *CVPR*, 2022. 2

[57] Shuling Zhao, Fa-Ting Hong, Xiaoshui Huang, and Dan Xu. Synergizing motion and appearance: Multi-scale compensatory codebooks for talking head video generation. In *CVPR*, 2025. 2

[58] Yufeng Zheng, Victoria Fernández Abrevaya, Marcel C Bühler, Xu Chen, Michael J Black, and Otmar Hilliges. Im avatar: Implicit morphable head avatars from videos. In *CVPR*, 2022. 2

[59] Yufeng Zheng, Wang Yifan, Gordon Wetzstein, Michael J Black, and Otmar Hilliges. Pointavatar: Deformable point-based head avatars from videos. In *CVPR*, 2023. 1, 2

[60] Zhenglin Zhou, Fan Ma, Hehe Fan, and Tat-Seng Chua. Zero-1-to-a: Zero-shot one image to animatable head avatars using video diffusion. In *CVPR*, 2025. 2

[61] Hao Zhu, Wayne Wu, Wentao Zhu, Liming Jiang, Siwei Tang, Li Zhang, Ziwei Liu, and Chen Change Loy. Celebvhq: A large-scale video facial attributes dataset. In *ECCV*, 2022. 1, 2

[62] Wojciech Zienonka, Timo Bolkart, and Justus Thies. Instant volumetric head avatars. In *CVPR*, 2023. 1, 2

[63] Wojciech Zienonka, Stephan J Garbin, Alexandros Lattas, George Kopanas, Paulo Gotardo, Thabo Beeler, Justus Thies, and Timo Bolkart. Synthetic prior for few-shot drivable head avatar inversion. In *CVPR*, 2025. 2

Generalizable and Animatable 3D Full-Head Gaussian Avatar from a Single Image

Supplementary Material

A. Preliminary

3D Gaussian Splatting (3DGS) [18] has gained recognition as a promising 3D representation, representing scenes with a collection of 3D Gaussians. Each Gaussian primitive has a series of attributes: the position $\mathbf{p} \in \mathbb{R}^3$, the scaling vector $\mathbf{s} \in \mathbb{R}^3$, the quaternion $\mathbf{q} \in \mathbb{R}^4$ representing rotation, the opacity $o \in \mathbb{R}$, and the color $\mathbf{c} \in \mathbb{R}^3$. The Gaussian is then defined as $\mathbf{G}(\mathbf{x}) = e^{-\frac{1}{2}(\mathbf{x}-\mathbf{p})^T \Sigma^{-1}(\mathbf{x}-\mathbf{p})}$, where $\Sigma \in \mathbb{R}^{3 \times 3}$ is the covariance matrix derived from \mathbf{s} and \mathbf{q} . Using a fast tile-based rasterizer, 3DGS enables real-time rendering.

FLAME [23] is a parametric face model that represents human face deformation by a combination of blendshapes and linear blend skinning (LBS), with parameters describing shape β , pose θ , and expression ψ . To deal with the deformation that LBS cannot model, additional blendshapes are applied to the template mesh vertices $\bar{\mathbf{V}}$ as:

$$\mathbf{V}_P = \bar{\mathbf{V}} + B_S(\beta; \mathcal{S}) + B_P(\theta; \mathcal{P}) + B_e(\psi; \mathcal{E}), \quad (11)$$

where $B_S(\beta; \mathcal{S})$, $B_P(\theta; \mathcal{P})$ and $B_e(\psi; \mathcal{E})$ represent shape, pose and expression blendshapes, respectively. Then, a standard skinning function W is utilized to produce the position of the deformed vertices \mathbf{V} :

$$\mathbf{V} = W(\mathbf{V}_P, \mathbf{J}(\beta), \theta, \mathcal{W}), \quad (12)$$

where \mathbf{J} is the joint locations, and \mathcal{W} is the blendweights.

B. Implementation Details

We use the FLAME model [23] with the mouth cavity covered following [45] as the parametric head model. We generate UV Gaussian attribute maps at $K^2 = 256^2$ resolution. To sample Gaussians from the UV Gaussian attribute maps, we use uniform grid sampling with a size of 256×256 , sampling one Gaussian from each UV map texel, except for the hair region, where we use the uniform grid of size 1024×128 to make Gaussians cover the back of the head more completely. We also sample the UV coordinates corresponding to the FLAME vertices. The sampling results in about 78K Gaussians. We extract $N = 4$ scales of the source image features for local UV feature extraction. In the symmetric UV space feature fusion module, We use 2 layers of the transformer block with convolution layers instead of linear layers to maintain the spatial structure of the UV map. The local window size w is set to 7.

During training, we randomly sample 2 inverted novel views in 3D reconstruction mode. We use the Adam optimizer with a learning rate of 1×10^{-4} . The model is trained with a batch size of 4 for 37500 iterations on one NVIDIA H800 GPU. The loss weights are set as $\lambda_{3d} = 50$, $\lambda_{eye} = 5$, $\lambda_{pos} = 1$, $\lambda_{shape} = 1$, $\lambda_{shape}^{tv} = 10$, $\lambda_{id} = 0.25$, $\lambda^1 = 0.5$, and the threshold is set to $\epsilon = 0.1$. We add \mathcal{L}_{3d} , \mathcal{L}_{eye} , \mathcal{L}_{shape}^{tv} and \mathcal{L}_{id} after training for 7500 iterations, and increase λ_{3d} to 100 after training for 25000 iterations.

C. Additional Details on Experiments

C.1. Additional Comparison Details

We compare our method with a group of open-source state-of-the-art methods, *i.e.*, the 2D-based StyleHEAT [49], the 3D-based GOHA [25], Real3DPORTRAIT [48], Portrait4D [8], Portrait4D-v2 [9], GAGAvatar [6] and LAM [14]. For each approach, we follow the official data pre-processing and animation procedures, and use the released checkpoint for evaluation.

C.2. Additional Experimental Results

C.2.1. Video Demos

We provide video demos on the project page². These video demos present results for comparison with state-of-the-art approaches in terms of avatar animation and full-head rendering. They demonstrate the effectiveness of our method, supporting high-quality animation and 360° rendering views.

C.2.2. Additional Qualitative Comparison Results

Full-Head Rendering. We compare the quality of full-head rendering with the 3D-based methods in Fig. 8. The avatar is animated by the driving motion before being rendered to different viewpoints across 360°. All other methods fail at large side or back views that significantly differ from the input source view, unable to model the back of the head. Only GAGAvatar [6] can roughly model the shape of the back head at side views, but the textures are coarse and contain visible artifacts. Meanwhile, due to its use of a 2D neural renderer on the rendered features, GAGAvatar cannot maintain 3D consistency of the face area under large camera pose changes. In contrast, by leveraging knowledge from the pre-trained 3D full-head GAN, our method reconstructs avatars with plausible details for the back of the head, improving the realism of animatable 3D head avatars.

²<https://shaelyn.github.io/fhavtar/>

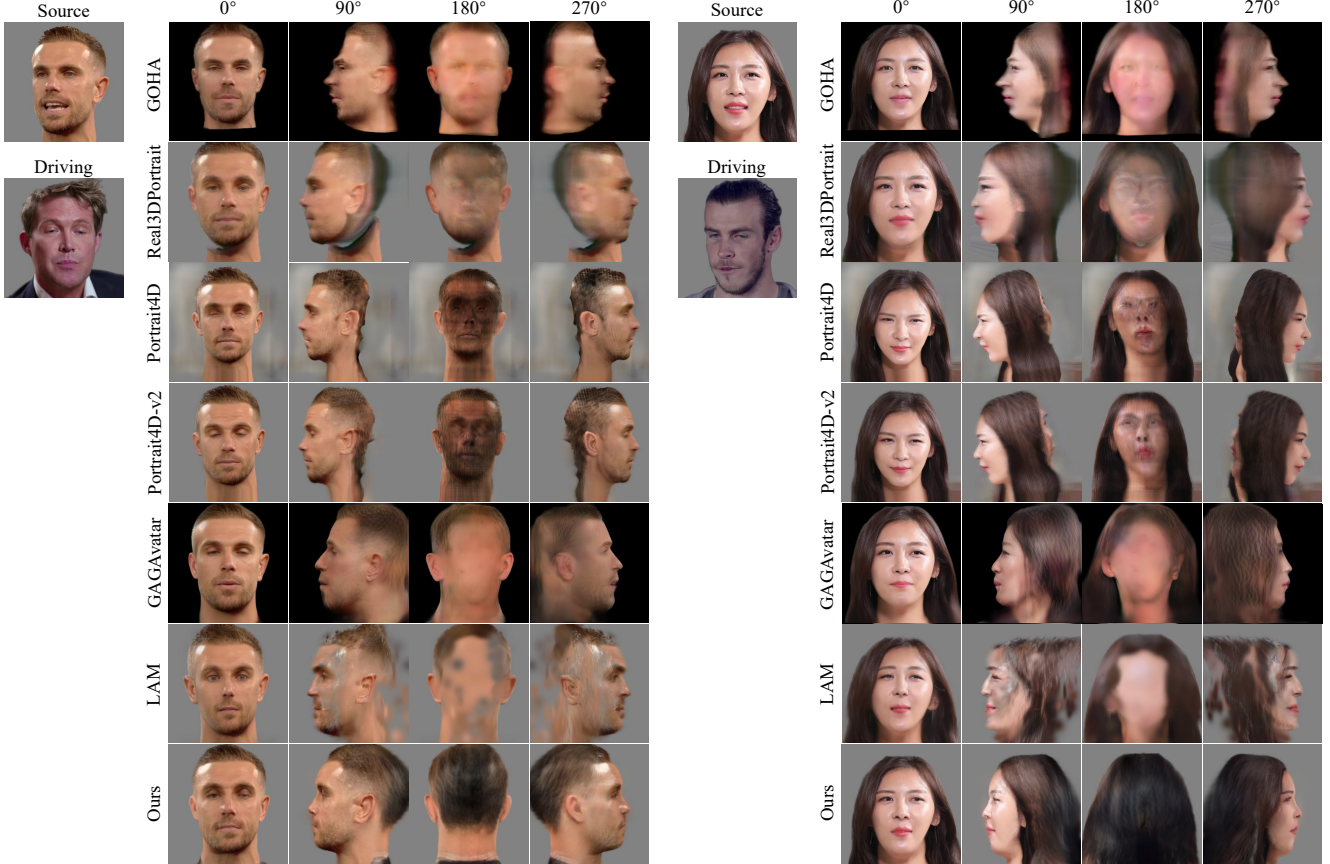


Figure 8. Qualitative comparison with state-of-the-art 3D-based methods (*i.e.*, GOHA [25], Real3DPortrait [48], Portrait4D [8], Portrait4D-v2 [9], GAGAvatar [6] and LAM [14]) for full-head rendering on the VFHQ [47] dataset. Our method renders plausible novel views across 360°, whereas other approaches fail at large side or back views.

Self-reenactment. We present qualitative comparison results for self-reenactment in Fig. 9. Our method can faithfully preserve appearance details in the source image and imitate the driving motion at the same time.

D. Limitations

Despite the capability of our method to generate animatable 3D full-head avatars, it still has several limitations that can be addressed in the future. First, our method cannot reconstruct accessories well, such as hats and glasses. The reason is that our method highly depends on the pre-trained 3D GAN and its inversion for global full-head feature extraction and novel view supervision, and the inversion method [2] is constrained by the latent space of the pretrained 3D GAN [1], which leads to noticeable artifacts when handling out-of-domain accessories, as shown in Fig. 10 (b) and (c). Besides, we obtain local UV feature maps by projecting points on the refined FLAME mesh to the 2D feature space, and the refined FLAME mesh cannot model glasses well, which makes our method treat glasses as textures on face surfaces, as shown in Fig. 10 (c). Sec-

ond, our performance on motion transfer is constrained by the estimated FLAME motion parameters. The limitation mainly comes from errors in the estimated parameters and the inability of FLAME to model certain motions, such as the tongue movement, as shown in Fig. 10 (e) and (f).

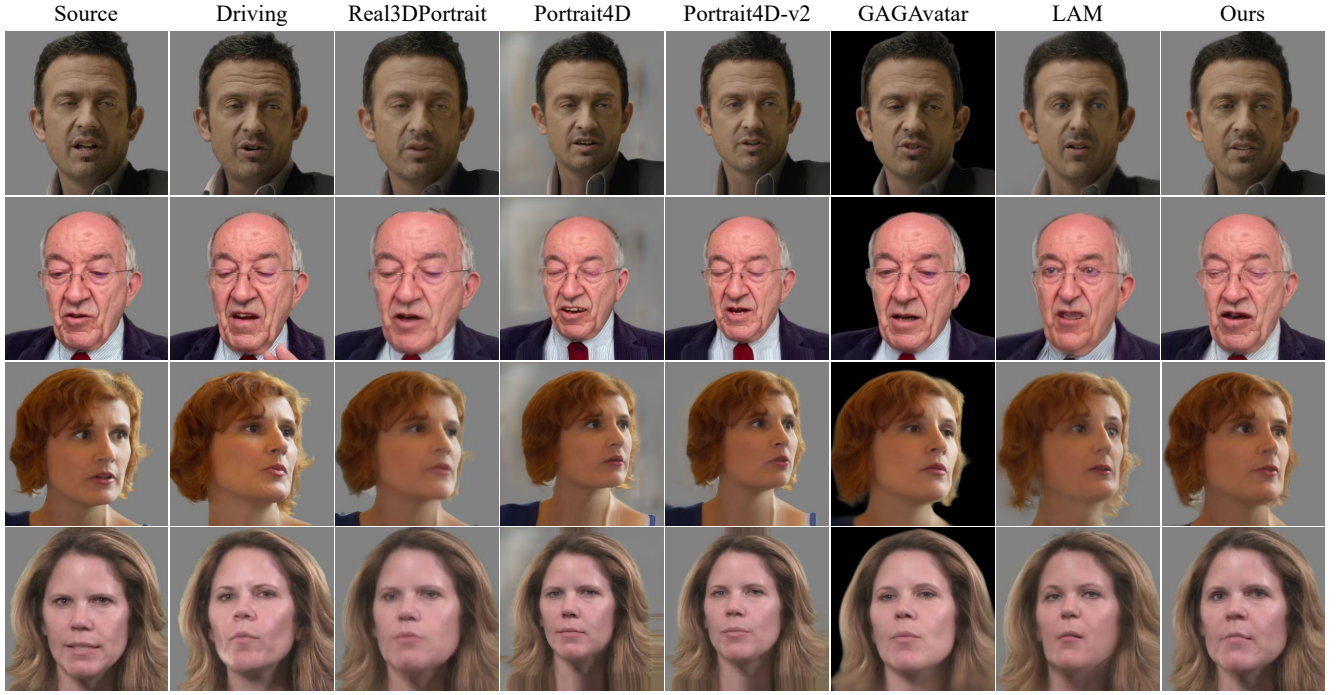


Figure 9. Qualitative comparison with state-of-the-art methods (*i.e.*, Real3DPortrait [48], Portrait4D [8], Portrait4D-v2 [9], GAGAvatar [6] and LAM [14]) for self-reenactment on the VFHQ [47] and HDTF [55] datasets. Our method best maintains source appearance details while effectively mimicking the driving motion.

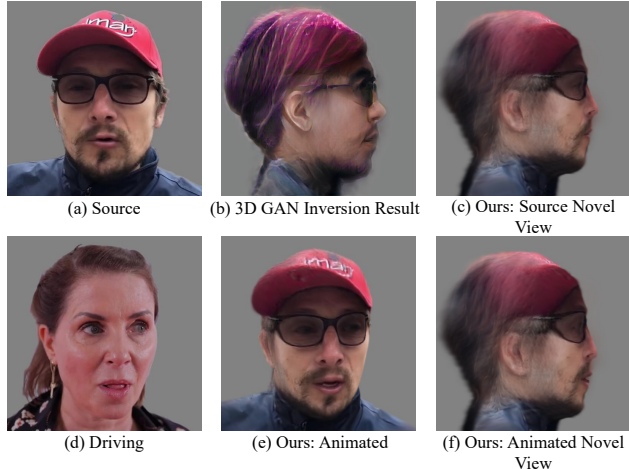


Figure 10. Failure cases of our method. It fails to reconstruct accessories faithfully and cannot transfer motions that FLAME cannot model, such as the tongue movement.